Science of the Total Environment 921 (2024) 171080

Contents lists available at ScienceDirect

Science of the Total Environment

journal homepage: www.elsevier.com/locate/scitotenv

Understanding drought propagation through coupling spatiotemporal features using vine copulas: A compound drought perspective

Guibin Yang, Jianxia Chang *, Yimin Wang, Aijun Guo, Lu Zhang, Kai Zhou, Zhenwei Wang

State Key Laboratory of Eco-hydraulics in Northwest Arid Region of China (Xi'an University of Technology), Xi'an 710048, China

HIGHLIGHTS

- Compound duration and compound area for quantifying spatiotemporal accumulation scale of drought propagation were proposed
- Evaluation lacking spatiotemporal information may underestimate drought propagation with low-I_{MD} but long-*CD* or large-*CA*
- The Vine copula can couple dependence relationships of compound drought characteristics and exhibits reliable robustness

GRAPHICAL ABSTRACT

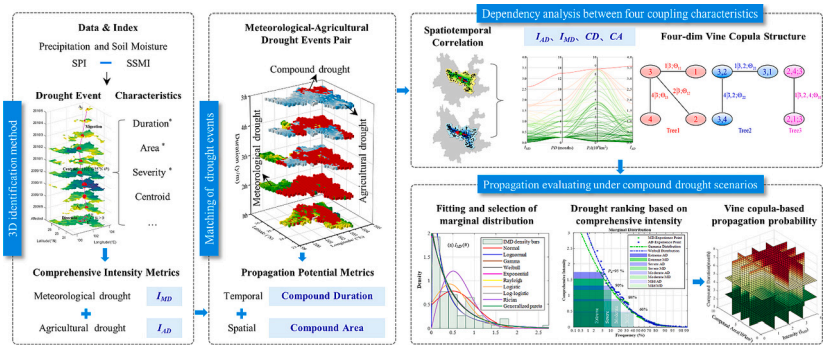

ARTICLE INFO

Editor: Ouyang Wei

Keywords:
Compound drought
Drought propagation
Vine copula
Propagation probability
3D-drought event
Compound duration and area

ABSTRACT

Accurately evaluating drought impact on agriculture poses a challenge to regional food security, particularly in compound drought (i.e., meteorological and agricultural drought co-occurring) scenarios. This study presents a novel approach utilizing Vine copula for coupling spatiotemporal features to evaluate drought propagation. Three-dimensional clustering method was employed to identify meteorological and agricultural drought events, which excelled in capturing dynamic evolution characteristics (duration, area, severity, etc.) as well as integrating them into comprehensive meteorological drought intensity (I_{MD}) and agricultural drought intensity (I_{AD}). Through spatiotemporal matching, compound drought events were extracted from the meteorological-agricultural drought event pairs. From compound drought perspective, compound duration (*CD*) and compound area (*CA*) were devised to characterize drought propagation potential across time and space. Finally, the Vine copula method was employed to model the interdependence between four key coupling features, namely I_{MD}, I_{AD}, *CD*, and *CA*, and evaluate the probability of triggering agricultural drought with different intensity levels. Results showed that *CD* and *CA* can respectively characterize the temporal and spatial accumulation scale of drought propagation. At a certain I_{MD} level, *CD* significantly influences the propagation probability (i.e., "stratification" phenomenon), while *CA* increases the probability proportionally. Probability evaluation lacking spatiotemporal information may underestimate the likelihood of drought propagation characterized by "low-I_{MD}" but "long-*CD*" or "large-*CA*". The four-dimensional Vine copula structure can effectively couple dependence relationships of compound drought characteristics, and exhibits reliable robustness. This research provides

* Corresponding author.
E-mail address: chxiang@xaut.edu.cn (J. Chang).

https://doi.org/10.1016/j.scitotenv.2024.171080
Received 7 November 2023; Received in revised form 1 February 2024; Accepted 16 February 2024
Available online 20 February 2024

stakeholders accurate probabilistic evaluation under compound drought scenarios, offering new insight into drought propagation.

1. Introduction

Global water cycle intensification, due to the combined effects of climate change and increased human activities, has accelerated drought escalation since the 1950s (Pascolini-Campbell et al., 2021; Walker and Van Loon, 2023). Droughts of the 21st century have impacted countries and regions worldwide to varying degrees (Biondi and Meko, 2019; Crausbay et al., 2017). For instance, the autumn-winter-spring drought in Southwestern China in 2009 (Liu et al., 2023a), California's protracted drought from 2012 to 2015 (Shi et al., 2021), Europe's high-temperature drought in 2018 (Zscheischler and Fischer, 2020), and the record-breaking global heatwaves and flash droughts in 2022 (Tripathy and Mishra, 2023). These severe droughts are compound in nature (AghaKouchak et al., 2020), occurring simultaneously with two or more drought types and characterized by prolonged duration, expansive scale, and extreme intensity.

Drought can be categorized into four types: meteorological drought, agricultural drought (also called soil moisture drought), hydrological drought, and socio-economic drought (Mallya et al., 2015). Compound drought broadly defined as the combination of two or more drought types leading to cascading impacts on natural and/or social systems (AghaKouchak et al., 2020). Precipitation deficit (meteorological drought) and soil moisture imbalance (agricultural drought) coinciding in time and space result in compound drought, triggering widespread vegetation mortality that profoundly impede the continent's capacity to serve as a carbon sink (Novick et al., 2016; Wu et al., 2022; Zhou et al., 2019). By late-21st century, probability, extent and severity of compound drought increase by 60 %, 10 % and 20 % relative to late-20th century (Singh et al., 2022). According to relevant research, from 1978 to 2018, drought had the most severe impact among major agro-meteorological disasters in China, with an average annual coverage area of 2.22 million hectares (Xu and Tang, 2021). Thus, this article specifically refers to compound drought as the co-occurrence of meteorological and agricultural drought, which has cascading effects on ecological environment and economic growth. Addressing this issue poses importance for tackling natural and societal challenges ahead.

Compound drought exhibits distinct spatiotemporal heterogeneity and coupling feature across diverse spatiotemporal scales (Vogel et al., 2021). In recent years, compound drought has gradually become a focal point of researchers' attention. However, the current understanding of compound drought needs further enhancement, and the intricate coupling mechanisms of various drought types remain inadequately understood (Wang and Yuan, 2022). For instance, the spatiotemporal coupling processes and key influencing factors of the transition from meteorological drought to agricultural drought. Elucidating the spatiotemporal coupling feature between meteorological and agricultural drought in compound drought scenarios is more crucial. Essentially, compound drought is the result of drought propagation (Eltahir and Yeh, 1999). Specifically, precipitation deficit causing meteorological drought depletes soil moisture, while sustained high temperatures increase evapotranspiration, exacerbating soil moisture loss and subsequently triggering agricultural drought (Jaranilla-Sanchez et al., 2011; Mishra et al., 2015). Drought propagation denotes the alteration of the drought signal as it traverses the terrestrial component of hydrologic cycle, involving the process by which meteorological drought transitions to agricultural drought (Van Loon, 2015; Zhang et al., 2022b). Conducting research on drought propagation could aid in deciphering the spatiotemporal coupling mechanism of compound drought, providing agricultural drought warning.

Related research has investigated drought propagation from multidimensional perspectives. Analytical methods can be categorized into physical simulation and statistical analysis (Zhou et al., 2021). Statistical approach of drought propagation focuses on the correlation, lag time, and influence factors across various spatiotemporal scales (Zhang et al., 2022a). Employing correlation analysis, Liu et al. (2023c) demonstrated that the transmission time from meteorological to agricultural drought globally averages 5.7 months. Xu et al. (2021) found that within China, this transmission spans 1–7 months. In temperate high-altitude zones, drought propagation is prolonged, increasing the likelihood of vegetation loss and extending recovery times beyond 7 months (Wu et al., 2024). Furthermore, the spatial density and persistence of drought are identified by Lin et al. (2023a) as more influential on drought propagation than its duration, area, and severity. Consequently, climate, elevation, and land use all impact drought dissemination (Liu et al., 2023d). Integrated consideration of these factors offers a more comprehensive assessment of drought propagation dynamics. In academia, probabilistic methods have been extensively researched and applied for assessing drought propagation. Multivariate analysis widely applied in drought studies owing to drought's multidimensional nature (Feng et al., 2019). Numerous studies aimed to incorporate multivariate meteorological characteristics to jointly assess the probability of drought propagation.

Nevertheless, previous research has divided the propagation process into temporal and spatial components, while neglecting the spatiotemporal link of drought features (Dobson et al., 2020; Tian et al., 2022). Insufficient attention has been paid to the spatiotemporal coupling alteration of the drought characteristics, especially in compound drought scenarios. In fact, when compound drought occurs, there is a feedback interaction between the characteristics of meteorological and agricultural drought events. Drought propagation is subject to the coupling effects of meteorological conditions, watershed characteristics, and land use (Apurv et al., 2017). Propagation probability depends not only on the intensity of a single event but also closely on propagation conditions, like the spatiotemporal boundaries (Lin et al., 2023b). Propagation process under compound drought scenarios constitute a high-dimensional problem (Ayantobo et al., 2021; Zhu et al., 2021). Traditional methods separate the spatiotemporal nature of propagation, neglecting their joint–dependent–occurrence, which may lead to uncertainty or erroneous calculations of propagation probabilities in larger spatial areas (Jehanzaib et al., 2020).

To address the high dimensionality, this study took into account the nonlinear relationships between the multidimensional characteristics of drought events, such as area, duration, and intensity, to propose comprehensive intensity metrics (I_{MD} for meteorological and I_{AD} for agricultural drought). Three-dimensional (3D) identification method was employed to determine the spatiotemporal structure of drought events from three dimensions: longitude, latitude, and time (Lloyd-Hughes, 2012; Weng et al., 2023). It allows for the extraction of spatiotemporally continuous compound drought events from pairs of meteorological and agricultural drought events. To consider spatiotemporal condition, two propagation potential metrics, compound duration (*CD*) and compound area (*CA*), were proposed from compound drought perspective. To evaluate drought propagation by integrating these spatiotemporal features, this study developed a propagation probability model utilizing Vine copula. The Vine Copulas have garnered researchers' widespread interest due to their flexible, simple structure and independence from marginal distributions of variables, making them suitable for modeling complex relationships among multivariate variables (Kanthavel et al., 2022; Thong et al., 2019). It can effectively couple the dependence structure of multivariate random variables (e.g., linear, nonlinear and tail dependence) and have been used for drought prediction (Wu et al., 2021), drought risk evaluation

(Nikraftar et al., 2021), drought indices establishment (Kanthavel et al., 2022; Kao and Govindaraju, 2010) and drought response analysis (Farrokhi et al., 2021). Thus, this study utilized four-dim Vine copula to model the dependency relationship between I_{MD}, I_{AD}, CD, and CA, and further evaluate the propagation probability from meteorological drought to agricultural drought.

The study's novelty lies in proposing comprehensive intensity metrics for drought events and propagation potential metrics under compound drought scenarios, and developing a Vine copula-based propagation probability model that couples spatiotemporal information to evaluate the likelihood of agricultural drought occurrence across diverse scenarios. The aim is to elucidate the dependence relationships among four key propagation features, namely I_{MD}, I_{AD}, CD, and CA, and to calculate the probability of triggering agricultural drought at different intensity levels. It aids in understanding and addressing the high dimensionality and multivariate non-linear relationships in drought propagation. The remainder of this paper is organized as follows: Section 2 describes the study area, data sources, and methodology; major findings and discussions are presented in Section 3; and conclusions are elucidated in Section 4.

2. Data and methodology

2.1. Study area and data

2.1.1. Study area

Central Yunnan (CY), situated in Yunnan Province, China, serves as the economic nucleus (Fig. 1). It spans an area of approximately 86,800 km^2, ranging between 99°27′E–104°15′E and 23°03′N–26°45′N. The region has a typical subtropical monsoon climate, with an annual mean precipitation of 982 mm. The whole year can be divided into rainy and dry seasons, with the dry season lasting from November to April, accounting for merely 15 % of the annual precipitation. Grain production in CY comprises one-third of the total output for Yunnan Province, rendering the region highly vulnerable to recurring drought events that cause substantial agricultural damages annually (Ma et al., 2021). For instance, this region experienced a severe 100-year compound drought during autumn, winter, spring, and early summer since the autumn of

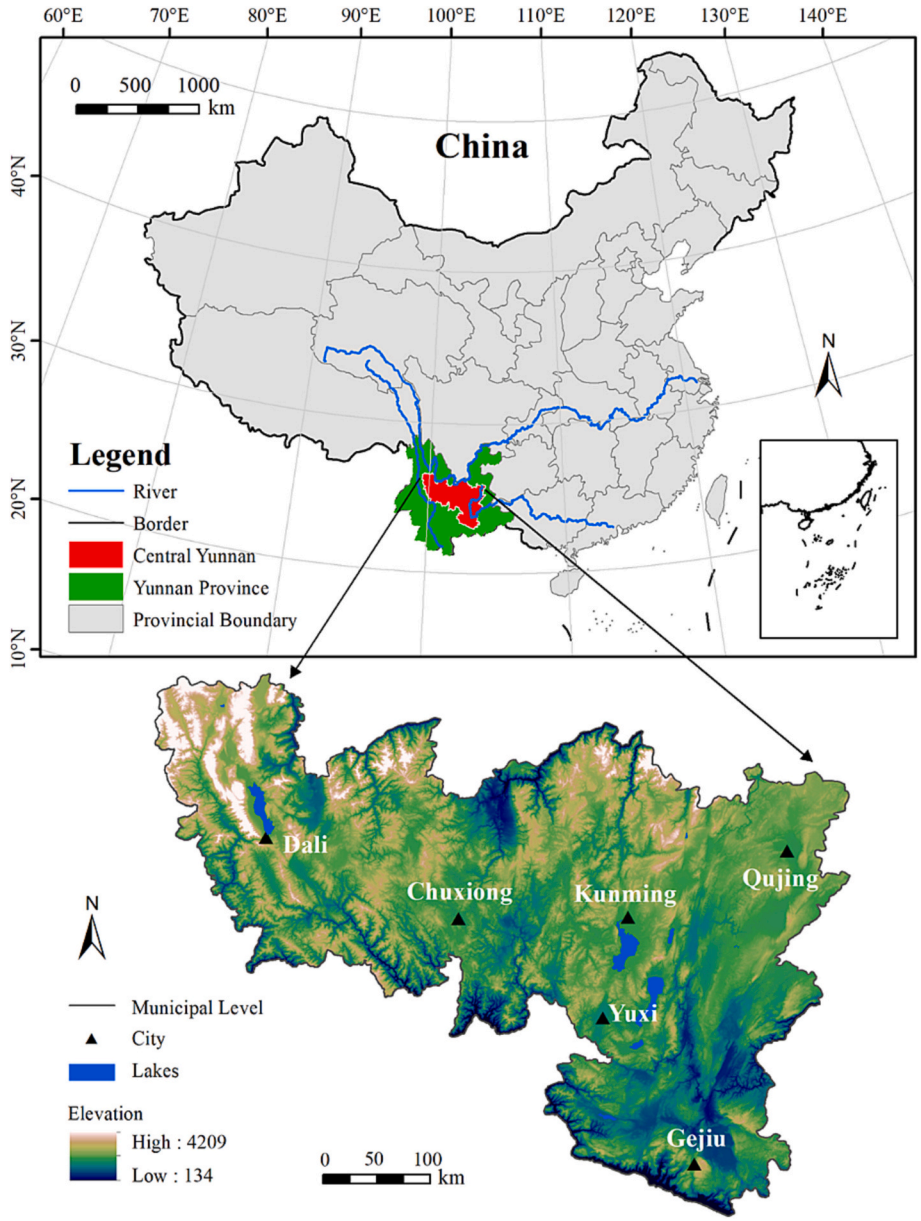

Fig. 1. Location and elevation distribution of CY.

2009, affecting half of its population and causing a 50 % decline in spring grain production (Liu et al., 2023b). Karst landforms, characterized by extensive soil and water erosion, exhibit high susceptibility to anthropogenic disruptions and climate change, especially to drought suppression. As a result, agriculture in these areas is vulnerable to drought due to its special location, Karst landforms, climate and geology. Evaluating drought impact on agriculture system in this typical drought-sensitive agricultural area provides new ideas and perspectives applicable to other global areas.

2.1.2. Data

This study utilized the Famine Early Warning Systems Network (FEWS NET) Land Data Assimilation System (FLDAS) (McNally et al., 2022) as data source to compute various drought indices. The FLDAS was developed as a collaboration between the U.S. Geological Survey (USGS) Earth Resources Observation and Science (EROS) Center, NASA Goddard Space Flight Center (GSFC), and others under the NASA Applied Sciences Program Water Resources project. The FLDAS dataset boasts exceptional spatiotemporal resolution, diverse variables, and reliable accuracy (Yu et al., 2023). It is widely applied in the evaluation of regional drought and food security (Li et al., 2020). The FLDAS data has a spatial resolution of 0.10° and consists of monthly time series spanning from January 1982 to present. Monthly FLDAS datasets for precipitation and soil moisture were acquired from NASA Goddard Earth Science Data and Information Service Center (GES DISC) to serve as original data for this study.

2.2. Methodology

2.2.1. Drought index and 3D-drought event identification

The standardized precipitation index (SPI) has various temporal scales (McKee et al., 1995). In this research, SPI3 with a closer correlation to agricultural drought was chosen to characterize meteorological drought. Three steps to calculate SPI are described as following:

Step 1: Construction of precipitation series and fitting of probability distribution function.

Step 2: Estimation of cumulative probability. For a given precipitation amount x_0, the modified probability that a random variable $\underline{x} < x_0$ can be calculated as Eq.(1):

$$P\left\{\underline{x} < x_0\right\} = q + (1-q)F(x_0) = q + (1-q)\int_0^{x_0} \frac{1}{\beta^{\gamma}\Gamma(\gamma)} x^{\gamma-1} e^{-x/\beta} dx \quad (x>0) \tag{1}$$

Herein, q is probability of no precipitation, and $F(x)$ represents the cumulative distribution function (CDF) of the random variable $\underline{x}$. The parameters β and γ are the scale and shape parameters of the gamma distribution, which can be estimated by the maximum likelihood estimation method.

Step 3: Transformation of cumulative probability to standard normal CDF. The SPI is the standard normal Z-value with zero mean and unit variance obtained from the quantile transformation.

The standardized soil moisture index (SSMI) is a dimensionless quantity used to monitor drought events and is one of the most effective indicators for evaluating agricultural drought (Liu et al., 2023b). We calculated the SSMI using soil moisture data at a depth of 10–40 cm from FLDAS to characterize agricultural drought.

$$SSMI_{i,j} = \frac{SM_{i,j} - \overline{SM_j}}{\delta_j} \tag{2}$$

where i is the range of years, j is the month between January and December, SM_{ij} and δ_j are the mean and standard deviation of soil moisture in month j, respectively.

Based on drought indicators (SPI & SSMI), a 3D clustering method is utilized to identify meteorological and agricultural drought events. This method can effectively capture the temporal continuity and spatial dynamic evolution characteristics of drought event. The primary procedural steps are as follows:

1) Identification of grid drought patches: Drought patches are identified using a run theory method, wherein a threshold value is selected to compare the drought index values of each grid point. Grid points surpassing the threshold are labeled as drought patches.

2) Extraction of spatial drought clusters: Spatially correlated drought patches within a specified time period are grouped into clusters using spatial clustering methods. In this study, grid point connectivity determines spatial relations, with a center grid point connected to its surrounding 8 points. Connected drought patches form the same drought cluster.

3) Temporal connection of drought clusters: Temporally related drought clusters coalesce into cohesive drought events. This study utilizes the overlap area between neighboring monthly drought clusters as a threshold to evaluate temporal correlation. If the overlap surpasses the threshold (A_0), the two drought clusters are regarded as part of the same drought event; otherwise, they are treated as separate drought events. A_0 was determined through sensitivity analysis.

2.2.2. Spatiotemporal characteristics and comprehensive intensity measurement

Based on the 3D identification method, this study constructs multi-dimensional characteristics to depict the occurrence and development process of 3D-drought event (Fig. 2a), including:

1) Drought duration (D, months) is defined as the time interval the initiation and termination of a drought event within the specified temporal scale.

2) Proportion of drought-affected area (A, %) is the ratio of the accumulated projected area of 3D-drought event on the longitude-latitude plane to the total area of the region.

$$A = \frac{A_1 \ldots \cup A_d \ldots \cup A_D}{A_{total}} \tag{3}$$

where: A_d represents the affected area of drought in the d^{th} month, and A_{total} is the total area of the region.

3) Drought relative severity (S) is the spatiotemporal average of the drought index relative to the baseline SPI during the drought period. It is a dimensionless index that represents the severity of drought.

$$S = -\frac{1}{NT}\sum_{d=1}^{D}\sum_{n=1}^{N}\left(SPI_{d,n} - S_0\right) \tag{4}$$

where: $SPI_{d,n}$ is the drought index for the n^{th} pixel in the d^{th} month during a drought event, and N is the total number of drought-affected pixels in the d^{th} month. S_0 is the baseline SPI, set at −0.5.

4) Drought spatial-temporal centroid (X_c, Y_c, T_c) characterizes the central location of a drought event (Rulinda et al., 2012). Weighted averaging of drought intensity values can be used to calculate the spatial-temporal centroid coordinates of a 3D-drought event.

$$X_c = \frac{\sum_{k=1}^{K}\sum_{d=1}^{D} S_{kd}x_{kd}}{\sum_{k=1}^{K}\sum_{d=1}^{D} S_{kd}}, Y_c = \frac{\sum_{k=1}^{K}\sum_{d=1}^{D} S_{kd}y_{kd}}{\sum_{k=1}^{K}\sum_{d=1}^{D} S_{kd}}, T_c = \frac{\sum_{k=1}^{K}\sum_{d=1}^{D} S_{kd}d}{\sum_{k=1}^{K}\sum_{d=1}^{D} S_{kd}} \tag{5}$$

where: The centroid coordinates (X_c, Y_c, T_c) represent the longitudinal, latitudinal, and temporal centers of the c^{th} drought event, where S_{kd} is the intensity value of the k^{th} grid point in the d^{th} month, and x_{kd}, y_{kd} represent the longitude and latitude coordinates of the grid point. D is the total duration, and K is the number of grid points that experienced drought in the d^{th} month.

5) Drought migration direction (θ, °) refers to the movement direction of the centroid between the start and end of the event, determined by orientations relative to the origin. The origin in Fig. 3a represents the centroid of study area, r denotes the radius from centroid to drought

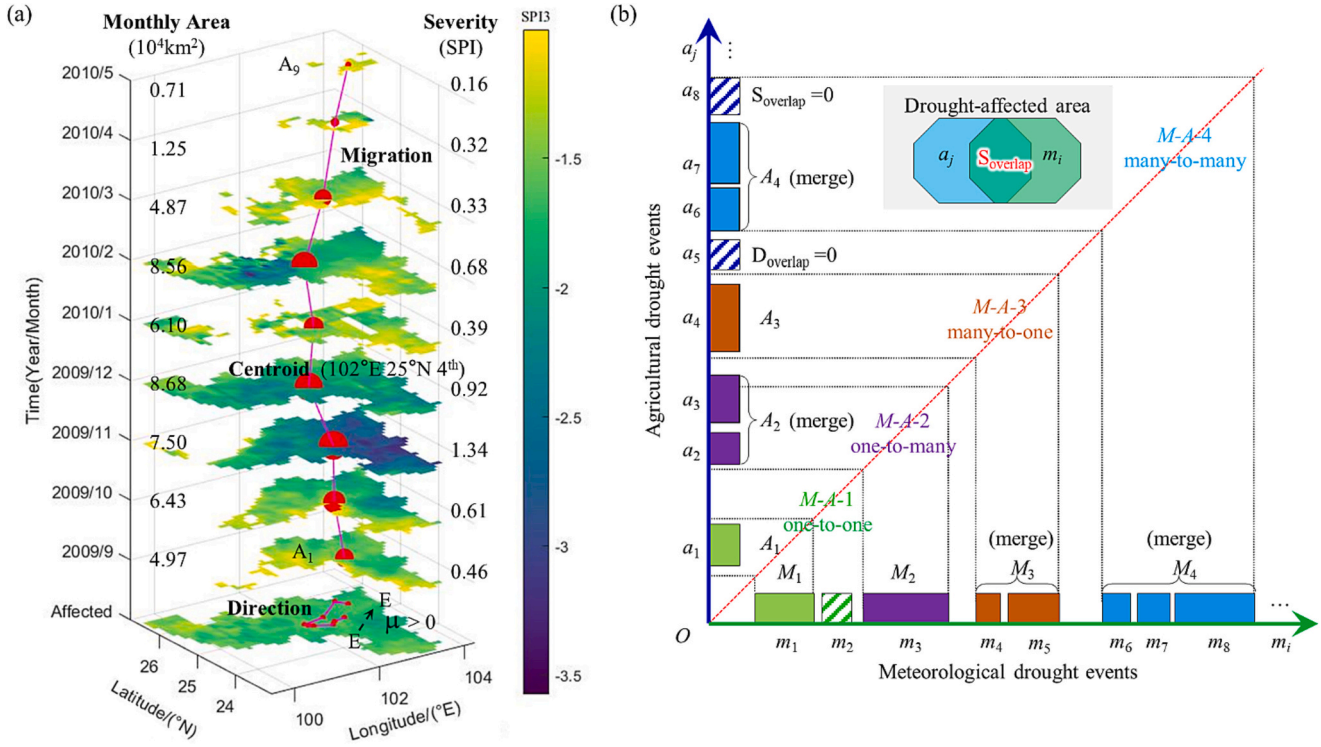

Fig. 2. (a) Schematic diagram of 3D-drought events and characteristics (taking the 2009 drought event as an example). (b) Schematic diagram of matching drought events based on spatiotemporal overlap criteria. Here, rectangles of the same color depict drought events with spatiotemporal overlap, while those without overlap feature diagonal shading.

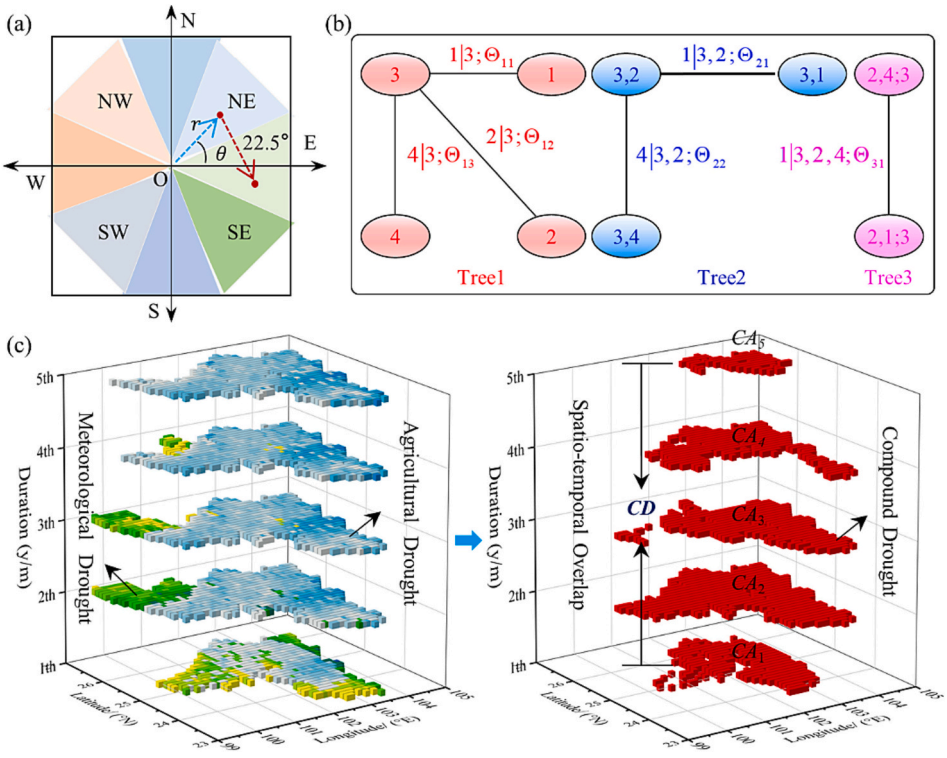

Fig. 3. (a) Schematic diagram of determination of drought migration direction. (b) Graphical model of a four-dimensional C-Vine copula. Here, each ellipse denotes a node and edge denotes bivariate copula density with abbreviated form and parameter(s) Θ. For example, "1|3" refers to c($u_1|u_3$) conditional copula, "1|3,2" refers to c ($u_1|u_3$, $u_2|u_3$) conditional copula, and Θ_{21} denotes parameters for the first edge of the second tree. (c) Schematic illustrating extraction of compound drought event from successfully matched drought event.

centroid, and θ represents the angle between drought centroid and positive x-axis. Eight orientations are considered in this study, with NE representing the orientation when $22.5^\circ < \theta < 67.5^\circ$. If the centroid orientation of a drought event is NE at the beginning and E at the end, then the migration direction is from NE to E (NE → E).

6) Drought precession characteristic μ describes the dynamic migration feature of the drought event in the circumferential direction. It is obtained by calculating the area of the polygon using the centroid coordinates X and Y as vertex coordinates. When $\mu > 0$, the overall drought migration exhibits a clockwise rotation feature.

$$\mu = (X_1 - X_D)(Y_1 + Y_D) + \sum_{d=1}^{D-1}(X_{d+1} - X_d)(Y_{d+1} + Y_d) \tag{6}$$

where: X_d and Y_d represent the longitude and latitude coordinates of the centroid of drought for the d^{th} month, respectively.

The relation of the Extreme-Intensity-Duration-Region (EIDR) comprehensively considers the nonlinear relationship among the duration, area, and severity of extreme disaster events and has been applied in monitoring regional precipitation events (Lu et al., 2017). To evaluate the intensity of 3D-drought events in terms of their spatial-temporal attributes, this study introduces a comprehensive intensity metric. This metric can be expressed as:

$$I = S^* D^{a^*} A^b \tag{7}$$

wherein: Parameters a and b are weighting coefficients ranging from 0 to 1, which can be estimated from multi-annual observations via linear regression (Lu et al., 2015). Small variations of the parameters around 0.5 have minimal impact on the relative ranking of the severity of extreme events and are commonly adopted (Lu et al., 2017). As such, the present study adopts values of $a = b = 0.5$.

Eq.(7) is applicable to various types of 3D-drought events. Within this article, I_{MD} and I_{AD} represent the comprehensive intensity metrics of meteorological and agricultural drought events, respectively. Compared to isolated drought characteristic like the S, the I_{MD} / I_{AD} metrics offer a more objective and comprehensive evaluation of drought impact by considering multidimensional drought features.

2.2.3. Matching 3D meteorological and agricultural drought events

To determine the propagation relationship between different drought types, this study employed a method based on spatiotemporal coincidence criteria to match meteorological and agricultural drought events. The methodology comprises the following steps:

Step 1: Arrange the identified 3D-drought events of both types chronologically. As shown in Fig. 2b, meteorological and agricultural drought events are denoted as m_i and a_j, respectively, according to their order of occurrence.

Step 2: Determine whether there is a temporal overlap between two drought events of different types using the Eq.(8):

$$D_{\text{overlap}} = \begin{cases} \neq \varnothing, & \begin{cases} MBT_i \le ABT_j \le MET_i \\ \quad or \\ ABT_j \le MBT_i \le AET_j \ \&\ \text{overlap} \ge min\left(DM_i/3DA_j/3\right) \end{cases} \\ = \varnothing, & \begin{cases} ABT_j > MET_i \\ \quad or \\ AET_j > MBT_i \end{cases} \end{cases} \tag{8}$$

where $D_{overlap} = \varnothing$ denotes no temporal intersection. The start and end times of the i^{th} meteorological and the j^{th} agricultural drought events are denoted as MBT_i, MET_i, ABT_j, and AET_j. Additionally, the duration of each meteorological and agricultural drought event is represented by DM_i and DA_j.

If temporal overlap exists, proceed to Step 3. Otherwise, no propagation relationship exists between the two drought events, as illustrated by m_2 and a_5 in Fig. 2b.

Step 3: Assess spatial overlap between drought events of the two types using the Eq.(9):

$$S_{\text{overlap}} = \begin{cases} \neq \varnothing, & \left(AM_i \cap AA_j\right) \ge A_0 \\ = \varnothing, & \left(AM_i \cap AA_j\right) < A_0 \end{cases} \tag{9}$$

where $S_{overlap} = \varnothing$ indicates no spatial intersection. AM_i and AA_j represent the affected areas of the i^{th} meteorological drought and the j^{th} agricultural drought, respectively. A_0 is the minimum threshold of overlapping area.

If spatial overlap also exists, it indicates a propagation relationship between the two drought events, matching them as a pair of drought events (Yoo et al., 2022), as this blocks with the same color in Fig. 2b. Otherwise, they cannot be matched together if there is no spatial overlap, as illustrated by m_8 and a_8.

Successful matched drought event pairs could have four propagation relations: one-to-one, one-to-many, many-to-one and many-to-many (Jiang et al., 2023). If there are multiple events, they must be integrated, merged accordingly, and renumbered in chronological order. Integrated meteorological drought events are denoted as [M_1, M_2, …] and agricultural drought events as [A_1, A_2, …]. Successfully matched and integrated drought event pairs are denoted as M-A-k (k = 1, 2, …).

2.2.4. Compound drought events and propagation potential metrics

The spatiotemporal overlap part (i.e., meteorological and agricultural drought co-occurring) indicates that compound drought has occurred. Based on successfully matched drought events (M-A-k), k compound drought events and their characteristics can be extracted (Fig. 3c). The characteristics (D and A) of compound drought event reflect the potential of meteorological-to-agricultural drought propagation. Current research overlooks the spatiotemporal conditions of drought propagation. Based on this assumption, two metrics were developed based on compound drought characteristics to quantify the potential for propagation across time and space.

1) Compound duration (CD, months), indicating the duration of concurrent meteorological and agricultural droughts (i.e., the duration of compound drought), expressed as Eq. (10):

$$CD = max(TM_{ini}, TA_{ini}) - min(TM_{ter}, TA_{ter}) \tag{10}$$

where: max(TM_{ini},TA_{ini}) represents the latest initiation time of the meteorological or agricultural drought, and min(TM_{ter},TA_{ter}) denotes the earliest termination time of the meteorological or agricultural drought.

2) Compound area (CA, km^2), which is the area where meteorological and agricultural droughts occur simultaneously (i.e., the affected area of compound drought), expressed as Eq.(11):

$$CA = CA_1 \cup \ldots CA_k \ldots \cup CA_{CD} \tag{11}$$

Herein, CA_k (k = 1, …, CD) represents the overlapping area of meteorological drought and agricultural drought for a compound duration of k months.

In general, the CD reflects the persistence of meteorological drought influences on agriculture, while the CA indicates the extent of such impacts. Meanwhile, the longer the CD and the larger the CA, the greater the intensity of the induced agricultural drought. Spatiotemporal coupling index f can be defined as the product of CD and CA, i.e.

$$f = CD \times CA \tag{12}$$

Herein, f is used to characterize the magnitude of propagation potential. The correlation between these variables is detailed analyzed in Section 3.3.2.

2.2.5. Vine copula propagation probability model for coupled spatiotemporal features

Vine copula decomposes multivariate variables into bivariate copula pairs, effectively addressing high-dimensional and heterogeneous dependencies (Ni et al., 2020). Based on Sklar's theorem (Sklar, 1959), the joint distribution function of an n-dimensional variable can be expressed as Eq. (13):

$$F(x_1, \ldots, x_n) = C\{F_1(x_1), \ldots, F_n(x_n)\} = C(u_1, \ldots, u_n) \tag{13}$$

Herein, $u_m = F_m(x_m)$ represents the cumulative distribution function of the random variable x_m ($m = 1, \ldots, n$), and C is an n-dimensional copula function. The probability density function (PDF) of the Eq. (13) can be expressed as Eq.(14):

$$f(x_1, \ldots, x_n) = \prod_{m=1}^{n} f_m(x_m) \times \prod_{i=1}^{n-1} \prod_{j=1}^{n-i} c_{i,i+j|1:(i-1)} \left\{ F(x_i|x_1, \ldots, x_{i-1}), F\left(x_{i+j}|x_1, \ldots, x_{i-1}\right) \right\} \tag{14}$$

where $c_{i,i+j|1:(i-1)}$ represents the PDF of bivariate copula.

Conditional distribution function of the Eq.(13) can be expressed as Eq.(15):

$$F(x|\mathbf{v}) = \frac{\partial C_{xv_j|\mathbf{v}_{-j}}\left[F\left(x|\mathbf{v}_{-j}\right), F\left(v_j|\mathbf{v}_{-j}\right)\right]}{\partial F\left(v_j|\mathbf{v}_{-j}\right)} \tag{15}$$

Herein, v_j ($j = 1, \ldots, n$) is any component of the vector $\mathbf{v}$, $\mathbf{v}_{-j}$ represents the remaining vector obtained by removing v_j from $\mathbf{v}$, and $C_{xv|\mathbf{v}}$ represents the bivariate conditional copula function.

Vine copula utilizes multiple trees interconnected by nodes and edges to establish the vine architecture. The n-dimensional copula function comprises (n-1) trees and C_n^2 edges. C-vines and D-vines are prevalent among the various vine structures. C-vines are robust for constructing multivariate distributions (Nikraftar et al., 2021) and are the main focus of this study.

Coupling I_{MD}, CD, and CA, this study comprehensively considers spatiotemporal features related to drought propagation. These three variables are used as conditional variables to calculate the conditional probability of the occurrence of agricultural drought intensity (I_{AD}) at different levels under certain meteorological condition and propagation potential. Denoting I_{AD}, I_{MD}, CD, and CA as x_1, x_2, x_3, and x_4, respectively, as shown in the graphical model in Fig. 3b, the conditional distribution function of $F(x_1|\, x_2, x_3, x_4)$ can be expressed as:

$$F(x_1|x_2, x_3, x_4) = \frac{\partial C_{x_1x_4|x_2,x_3}\left[F_{x_1|x_2,x_3}(x_1|x_2, x_3), F_{x_4|x_2,x_3}(x_4|x_2, x_3)\right]}{\partial F_{x_4|x_2,x_3}(x_4|x_2, x_3)} \tag{16}$$

The function $h(x, \mathbf{v}; \Theta)$ is introduced to represent the conditional distribution function of x given $\mathbf{v}$, where $F_{x_1|x_2,x_3}(x_1|x_2, x_3) = \frac{\partial C_{x_1x_2|x_3}\left[F_{x_1|x_3}(x_1|x_3), F_{x_2|x_3}(x_2|x_3)\right]}{\partial F_{x_2|x_3}(x_2|x_3)} = h\{h(u_1|u_3; \Theta_{11})|h(u_2|u_3; \Theta_{12}); \Theta_{21}\}$. The Eq.(16). can be further expressed as follows:

$$F(x_1|x_2, x_3, x_4) = h\{h[h(u_1|u_3; \Theta_{11})|h(u_2|u_3; \Theta_{12}); \Theta_{21}] \\ |h[h(u_4|u_3; \Theta_{13})|h(u_2|u_3; \Theta_{12}); \Theta_{22}]; \Theta_{31}\} \tag{17}$$

Given i^{th} tree and j^{th} edge of the vine, Θ_{ij} represents the copula parameters of the bivariate copula.

Using the Eq.(17), the required conditional probability $F(I_{AD} \mid I_{MD}, CD, CA)$ can be calculated.

3. Results and discussion

3.1. Identified 3D-drought events and drought characteristics

Using the 3D identification method, 173 meteorological drought events based on SPI3 and 228 agricultural drought events based on SSMI were identified in CY from 1982 to 2021. Unique parameter A_0 was appropriately set to 1.5 % ~ 1.6 % of the total study area, consistent with current research (Yoo et al., 2022). Table 1 and Table 2 lists the 10 most severe drought events ranked by comprehensive drought intensity.

Results showed that 64.7 % of the total meteorological drought events and 71.9 % of the agricultural drought events had a drought duration of one-month or less, an impact area of < 18,000 km^2, and a drought intensity of < 0.4, indicating that CY was prone to short-duration, small-area, and mild drought events. The 3D identification method is effective in detecting minor drought events, consistent with the findings of Liu et al. (2019).

Based on the duration, the average duration of meteorological droughts was 1.8 months, while the average duration of agricultural droughts was 1.5 months. The longest meteorological drought (MNo.4) lasted for 10 months, while the longest agricultural drought (ANo.1) lasted for 12 months, both being the historical maxima (Ma et al., 2021; Wang et al., 2023). In terms of affected area, the average impact area of meteorological droughts was 18,500 km^2, while that of agricultural droughts was 15,900 km^2. The largest impact areas were MNo.1 and MNo.7 meteorological drought events, both covering an area of 86,800 km^2 and ANo.4 agricultural drought event covering an area of 86,300 km^2, with a coverage rate of 99.4 %. Notably, due to the lower frequency of meteorological drought events compared to agricultural drought events, the average duration, area, and intensity of meteorological droughts are greater. However, despite the seemingly lesser impact, the agricultural drought characteristics (e.g., duration) exhibit a wider range of variation, suggesting that the distribution of agricultural drought characteristics is more extreme.

According to Fig. 4, which shows the seasonal distribution of drought characteristics, meteorological droughts were most likely to occur in spring (53 events, 30.6 %) and autumn (49 events, 28.3 %), with an average duration of 1.8 and 1.7 months, and an average impact area of 22,420 km^2 and 14,750 km^2, respectively. Agricultural droughts were most likely to occur in spring (81 events, 35.5 %) and summer (53 events, 23.3 %), with an average duration of 1.3 and 2.0 months, and an average impact area of 16,070 km^2 and 18,530 km^2, respectively.

Table 1
Top 10 meteorological drought events and their characteristics in CY identified by 3D identification method.

No.	Initiation (y/m)	Termination (y/m)	Duration (m)	Area (10^4km^2)	Severity (#)	Intensity (#)	Spatial-temporal Centroid			μ (#)	Direction (#)
							X_c (°E)	Y_c (°N)	T_c		
1	2009/9	2010/5	9	8.68	0.58	1.74	102.41	25.03	4th	17.4	E→E
2	1992/5	1992/11	7	8.64	0.65	1.72	102.33	25.01	4th	−22.0	E→E
3	2011/5	2011/11	7	8.60	0.62	1.64	102.66	25.04	4th	−47.8	E→E
4	2012/7	2013/4	10	8.66	0.46	1.45	101.85	25.24	7th	48.82	NW→E
5	1983/5	1983/9	5	8.61	0.63	1.40	102.04	25.06	3th	−63.4	NW→NW
6	2020/11	2021/5	7	7.35	0.49	1.19	101.50	25.30	4th	−106.9	N→NW
7	2019/4	2019/6	3	8.68	0.67	1.16	102.19	24.88	2th	−30.9	E→NW
8	2015/5	2015/8	4	3.77	0.80	1.05	100.66	25.57	2th	−5.3	W→NW
9	2001/4	2001/5	2	4.51	0.95	0.97	101.34	25.63	1th	–	NW→NE
10	1985/10	1986/3	6	7.49	0.42	0.95	102.59	25.07	5th	14.27	N→E

Table 2
Top 10 agricultural drought events and their characteristics in CY identified by 3D identification method.

No.	Initiation (y/m)	Termination (y/m)	Duration (m)	Area (10^4km^2)	Severity (#)	Intensity (#)	Spatial-temporal Centroid			μ (#)	Direction (#)
							X_c (°E)	Y_c (°N)	T_c		
1	2009/10	2010/9	12	8.02	0.68	1.79	102.50	24.84	6th	−4.3	E→NE
2	2012/9	2013/4	8	8.58	0.62	1.75	101.97	25.10	5th	90.08	W→NE
3	2011/6	2012/1	8	8.21	0.61	1.68	102.60	25.08	4th	−55.92	E→NE
4	1992/6	1992/12	7	8.63	0.61	1.62	102.26	24.93	3th	138.3	W→NE
5	1983/4	1983/9	6	8.54	0.57	1.38	101.88	25.11	3th	−132.8	NE→NW
6	1989/7	1990/2	8	7.81	0.46	1.24	102.47	24.97	4th	20.38	NE→NE
7	2003/7	2004/1	7	8.61	0.45	1.20	102.39	25.02	4th	55.34	W→NE
8	2013/7	2014/2	8	7.28	0.43	1.10	102.02	25.24	1th	−107.6	E→NW
9	2012/1	2012/3	3	8.50	0.61	1.05	102.15	25.15	2th	37.77	NW→N
10	1993/4	1993/8	5	8.45	0.47	1.04	102.38	24.92	3th	−31.38	NE→W

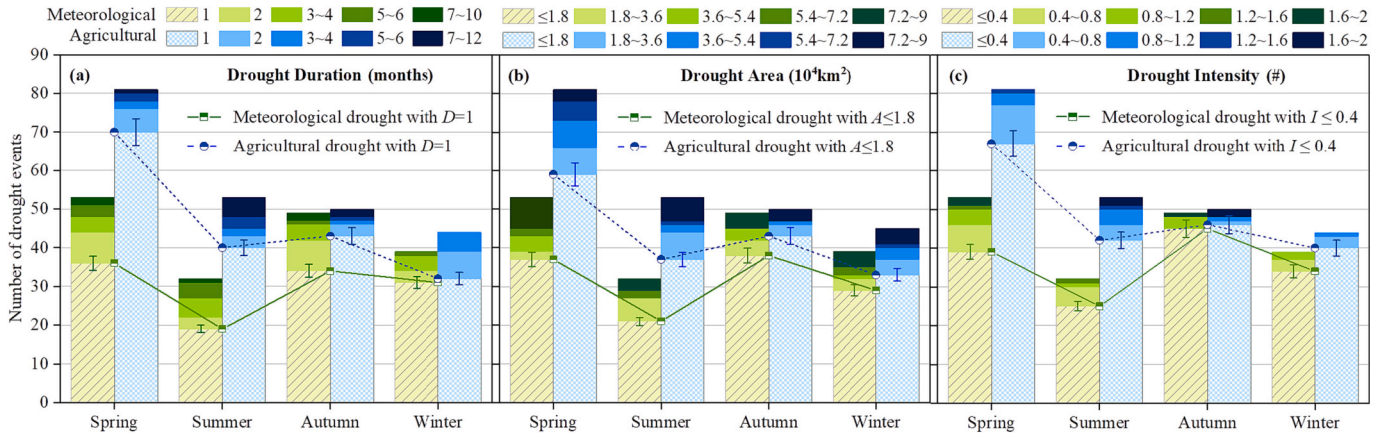

Fig. 4. Clustered stacked bar chart of drought characteristics in each season. (a) Drought duration, (b) Drought area, (c) Drought intensity. The *y*-axis is stacked by the number of drought events.

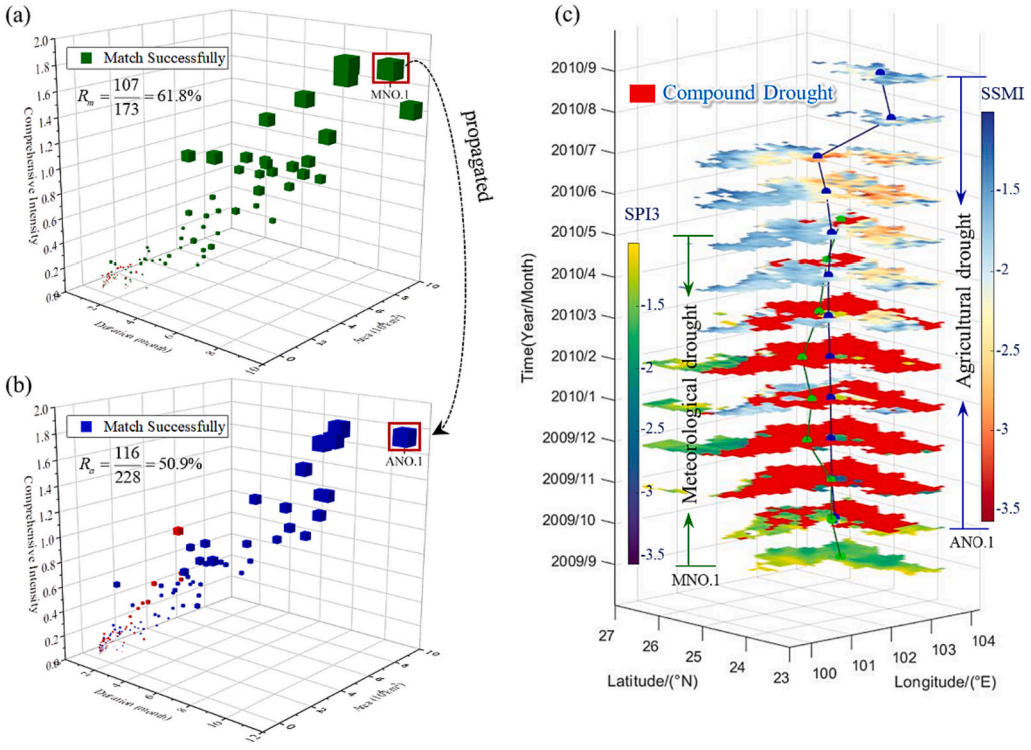

Fig. 5. Matching results of drought events. (a) Meteorological drought events. (b) Agricultural drought events. (Here, the red box represents unmatched drought events and "*R*" is the matched success rate). (c) Spatiotemporal continuity and propagation process of MNo.1 and ANo.1 under compound drought scenarios.

Consistent with Wang et al. (2021), results suggest that the drought-prone seasons in CY were concentrated during the crop growing season, which poses challenges for agricultural production.

3.2. Matched meteorological-agricultural drought events pairs

Based on the matching criteria in Section 2.2.3, 107 out of 173 meteorological drought events ($R_m = 61.8$ %) and 116 out of 228 agricultural drought events ($R_a = 50.9$ %) were successfully matched. Fig. 5a and b show the matched status of all meteorological and agricultural drought events. Results show that most drought events had been successfully matched, and the main reasons for matching failures were shorter duration, smaller area, and milder intensity. Although the failed matches of drought events were minor and did not significantly impact the results, they may still have contained valuable information related to propagation probabilities. However, this study did not enclose them within the scope of sampling.

One meteorological drought may trigger one or more agricultural droughts, and one agricultural drought may also be caused by multiple meteorological droughts. Accordingly, four situations materialized: one-to-one (55.1 %), one-to-many (17.9 %), many-to-one (16.7 %), and many-to-many (10.3 %). For non-single type drought events, a new drought event was formed through merging. The duration was defined as the period from the start of the first event to the end of the last event, while the intensity was calculated as the sum of all drought events' intensity values. The affected area was determined as the union of all drought events' impact areas. After merging, a total of 78 meteorological-agricultural drought event pairs (*M-A*-78) were assembled. It's important to note that merged matched drought pairs may overestimate drought intensity, necessitating caution in applying this approach (Gao et al., 2024).

Any pair of successfully matched drought events have complex propagation process. Analysis showed a one-to-one propagation relationship between MNo.1 and ANo.1 (as shown in the red boxes in Fig. 5a-b), taking them as typical drought event pair. Fig. 5c visualizes their monthly evolution and detailed propagation process. Results revealed that MNo.1 originated in Kunming City in eastern CY in autumn 2009, and after one month, ANo.1 was triggered at the same direction, and compound drought (where both MNo.1 and ANo.1 occurred) rapidly expanded. Their trajectories almost overlapped from September 2009 to February 2010, and both slowly migrated westward. While MNo.1 declined northwestward from November 2009 when its intensity peaked, ANo.1 did not immediately stop, but continued to develop until it receded to the southeast in July–September.

Sustained precipitation deficits in certain regions serve as potential factors triggering agricultural drought (Chang et al., 2016). Fig. 6a and b illustrate the monthly migration trajectories and drought area of MNo.1 and ANo.1, emphasizing the link between *CD* and CA. The transmission of meteorological drought to agricultural drought is achieved through a certain spatiotemporal accumulation mechanism. Propagation potential between these two drought types can be characterized by their spatiotemporal intersection, namely the characteristic *CD* and *CA* of compound drought. *CD* (8 months) reflects the cumulative effect of MNo.1 on the intensity of ANo.1, and *CA* (71,800 km^2) reflects the range of the intensity of MNo.1 on ANo.1. Findings revealed that meteorological drought of specific intensity (MNO.1) triggered agricultural drought (ANO.1) through distinct spatiotemporal cumulative effects. Therefore, *CD* and *CA* play a pivotal role in drought propagation, warranting consideration to unravel the underlying mechanism.

3.3. Dependency analysis between coupling characteristics

3.3.1. Spatiotemporal relationship

A spatiotemporal relationship existed between propagated drought events and that this could be quantified (Rulinda et al., 2013). The overall migration directions of the region's drought events were analyzed using ArcGIS. Fig. 7a and b show the drought centroids and their migration trajectories for each meteorological and agricultural drought event in CY, separately. The 173 meteorological drought events were dispersed throughout the CY, with an average drought centroid located in the middle of the region. The overall migration direction was from southeast to northwest (SE → NW). The average drought centroid of the 228 agricultural drought events was located slightly to the west of the meteorological drought, and their overall migration direction was similar. Results suggested that the overall migration and evolution patterns of meteorological and agricultural droughts in CY were consistent. Propagated drought event pairs exhibited a profound spatiotemporal correlation, warranting further in-depth analysis.

3.3.2. Correlation analysis between drought characteristics

The coupling characteristics of 78 pairs of propagated drought events were calculated, including I_{MD} for meteorological and I_{AD} for agricultural drought, as well as *CD* and *CA* as propagation potential features. Parallel coordinates in Fig. 8a visualize the characteristics of the 78 pairs of propagation drought events. As observed, the variables are concentrated in lower values, with 61.3 % of I_{MD} and 78.6 % of I_{AD} falling below 0.5. Meteorological drought with low-I_{MD} and short-*CD* was generally difficult to trigger high-I_{AD} agricultural drought. I_{MD} spread to I_{AD} through a special "channel", and *CD* and *CA* played a crucial role as the bridge in this propagation process.

Scatter plots were employed to investigate the qualitative correlation between *CD*, *CA*, *f*, I_{MD}, and I_{AD}. Fig. 8b analyzed the dependency of each

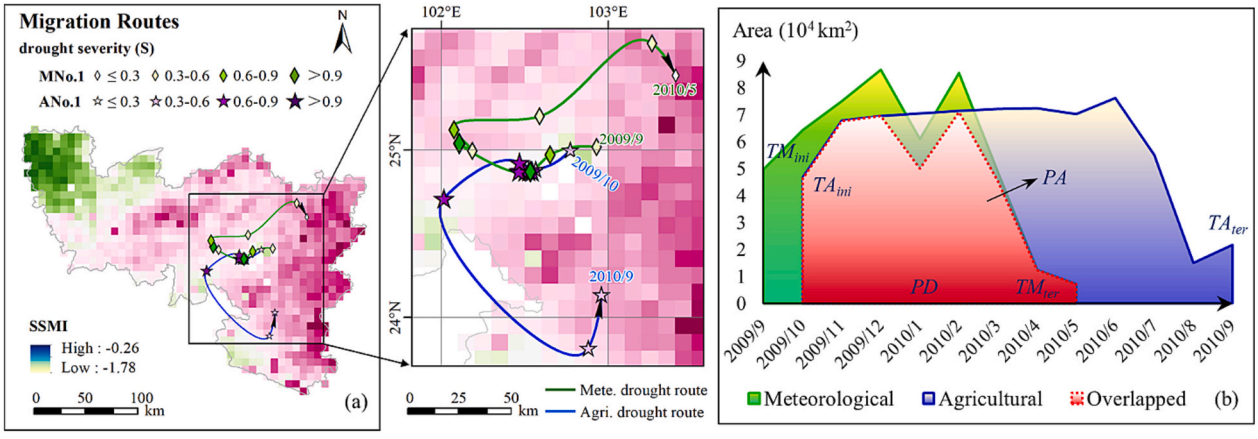

Fig. 6. Dynamic evolution of typical drought events MNo.1and ANo.1. (a) Migration route of drought centroid. (b) Evolution relationship between compound duration (*CD*) and compound area (*CA*).

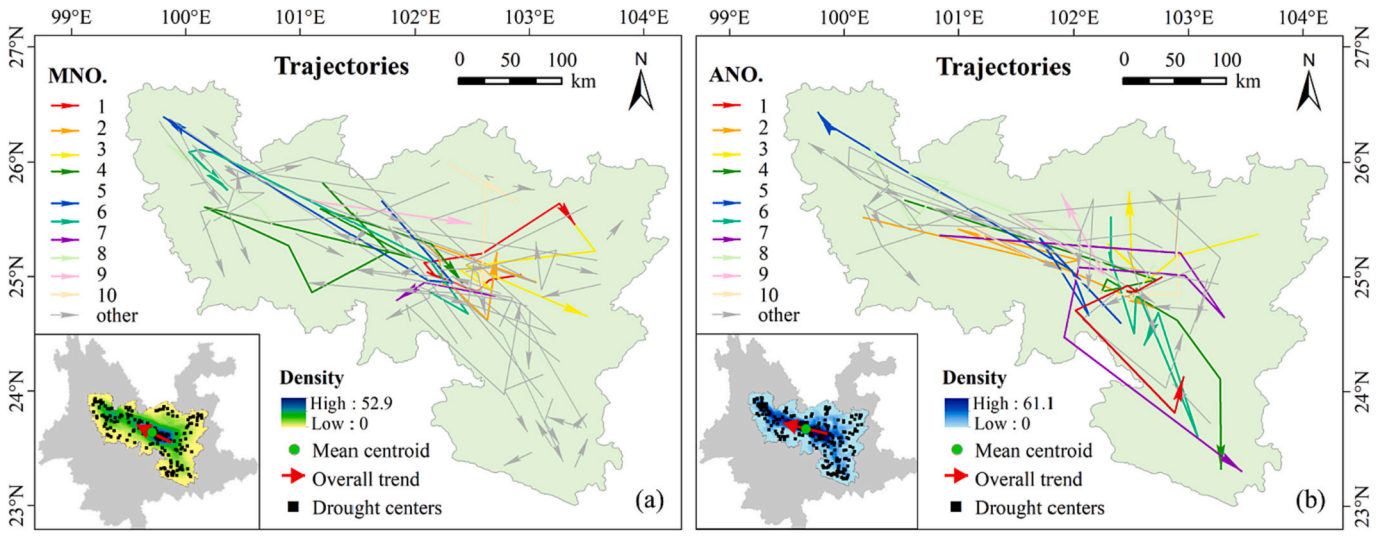

Fig. 7. The migration trajectories of top 10 meteorological drought (a) and agricultural drought (b) events in CY. Here, the drought centroid is located at a green point, and the overall migration trend is a red arrow.

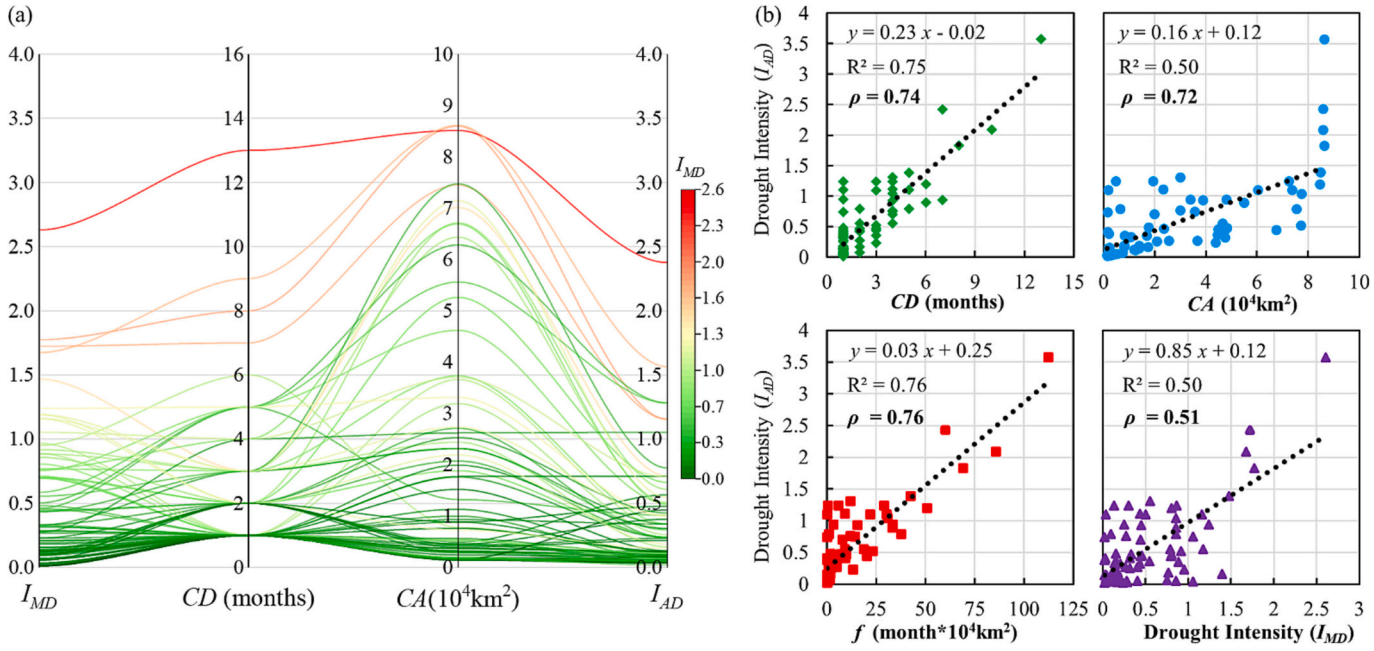

Fig. 8. (a) Parallel coordinate diagram of the coupling characteristics (I_{MD}, CD, CA, and I_{AD}) of 78 drought event pairs. (b) Scatter plot and correlation coefficient between I_{MD}, CD, CA, f, and I_{AD}.

variable with I_{AD}. Correlation analysis indicated that: (1) There was a positive correlation between each variable and I_{AD}, with a determination coefficient $R^2 \geq 0.5$, and most points clustered in the lower left corner. (2) At a 5 % significance level, the correlation coefficients demonstrated statistical significance, with the strongest correlation between variable f and I_{AD} (Spearman's $\rho = 0.76$). (3) The correlation coefficient between f and I_{AD} was greater than that between I_{MD} and I_{AD} ($\rho = 0.51$). Therefore, CD and CA encompassed probability information pertaining to subsequent agricultural drought. It was appropriate to couple CD and CA and model the joint distribution based on Vine copula function, as they had significant mutual dependence with agricultural drought.

Notably, the "unbalanced" distribution of sample points—where most sample points represent relatively mild drought events, while severe drought events account for only a small portion—results in most scatter points being concentrated in the lower left corner of the scatterplot. The correlation coefficients provided offer a general indication of the linear correlation between variables, but are insufficient to capture the complexity of their specific structures and causal relationships. Additionally, the *P*-values of statistical tests are influenced by statistical methods and sample sizes. Therefore, the specific structures of the Vine copula and the conditional dependencies between variables are further discussed in Section 3.3.3.

3.3.3. *Four-dim vine copula and conditional dependency*

In this study, the variables I_{AD} (x_1), I_{MD} (x_2), CD (x_3), and CA (x_4) were used for modeling a four-dimensional Vine copula conditional probability distribution, where x_1 was used as a predictor variable and x_2, x_3, and x_4 were used as conditional variables. The tree structure, nodes, and edge information of the constructed tree, selected based on the AIC criterion, are summarized in Table 3. The structure of tree is

Table 3
The structure of four-dimensional C-Vine copula.

tree	edge	copula	par	par2	τ_k	τ_u	τ_l
1	3,1	Joe copula	13.37* (0.01)	–	0.86	0.95	–
	3,4	Frank copula	5.07* (0.81)	–	0.46	–	–
	3,2	Joe copula	13.37* (0.01)	–	0.86	0.95	–
2	2,1;3	*t* copula	0.16* (0.05)	6.10* (0.74)	0.10	0.06	0.06
	2,4;3	Frank copula	1.88* (0.47)	–	0.20	–	–
3	4,1;2,3	Frank copula	1.18* (0.01)	–	0.13	–	–

Note: The copula functions include Gaussian copula, t-copula, Clayton copula, Gumbel copula, Frank copula, Joe copula and their rotated families. The par and par2 are parameters of the copula function. The "τ_k" is Kendall's tau coefficient. The "τ_u" is upper-tail dependence coefficient and the "τ_l" is lower-tail dependence coefficient. The symbol (*) denotes statistical significance at the 5 % level.

shown in Fig. 3b.

Analyzing the unconditional Vine copula structure (tree 1) reveals that the vine was constructed around *CD*, as indicated by the three edges sharing common node 3. *CD* (x_3) and I_{AD} (x_1) exhibit a positive correlation, suggesting prolonged compound duration could exacerbate the intensity of agricultural drought. Meanwhile, the upper-tail dependence suggested that a rapid increase in compound duration tend to coincide with synchronous increases in agricultural drought intensity, indicating a possible strong structural dependence between them. Similarly, there was a similar dependence between *CD* and I_{MD} (x_2).

Analyzing the higher-dimensional copula structure (tree 2 and tree 3) revealed additional propagation relationships of more indirect nature, as theoretically expected to decrease gradually with the increase of dimensionality. For instance, under the given conditions of I_{MD} and *CD*, the τ_k of *CA* and I_{AD} was only 0.13, potentially suggesting *CA* had a limited effect on the resulting agricultural drought. Nonetheless, more data would be needed to validate these exploratory findings, as meaningful inference about the dependency structure is difficult with the small number of samples.

3.4. Propagation evaluating under compound drought scenarios

3.4.1. Fitting and optimal selection of marginal distribution

Construct the joint distribution utilizing optimal marginal distributions. It is crucial to acknowledge that employing ill-suited distributions may lead to substantial errors (Zhang et al., 2021). This study considered 10 common distributions (Gamma, etc., Fig. 9a-d) as optional distributions. To alleviate the modeling uncertainties stemmed from different marginal distributions, only the best-fitting functions were employed for the modeling of I_{AD}, I_{MD}, *CD*, and CA. Maximum likelihood estimation was used to determine distribution parameters. Additionally, Kolmogorov-Smirnov (K-S) test was employed to assess the goodness-fit of different distributions. The K-S statistic serves as the criterion for determining the optimal distribution.

Table 4 summarizes the optimal distribution for each variable and the corresponding parameters for each distribution. Results indicate that I_{MD}, I_{AD}, and *CD* follow Gamma, Weibull, and Weibull distributions, respectively, while *CA* follows a Log-logistic distribution. After a probability integral transformation, marginal cumulative distribution function values *u* (between 0 and 1) required for calculating the probability of the Vine copula model can be obtained. Notably, this study assumes the variations of drought sequences and coupled variables within the research scope to be stationary, meaning their statistical properties do not undergo periodic changes due to external factors (such as the annual cycle of Earth). Additionally, as a prerequisite for data-based inference, the assumption of ergodicity is equally crucial as the assumption of stationarity. It enables this study to make probabilistic inferences utilizing the Vine copula model. Although we selected the optimal

Table 4
Goodness-fit of the optimal marginal distribution and its corresponding parameters (p = 5 %).

Variable	Distribution	K-S Test	Statistic	*P*-value	Parameters
$\boldsymbol{I_{MD}}$	Gamma	√	0.096	0.433	β = 0.944 γ = 0.532
$\boldsymbol{I_{AD}}$	Weibull	√	0.067	0.847	A = 0.527 B = 0.917
CD	Weibull	√	0.181	0.58	A = 3.461 B = 1.380
CA	Log-logistic	√	0.119	0.206	ε = 0.293 σ = 0.859

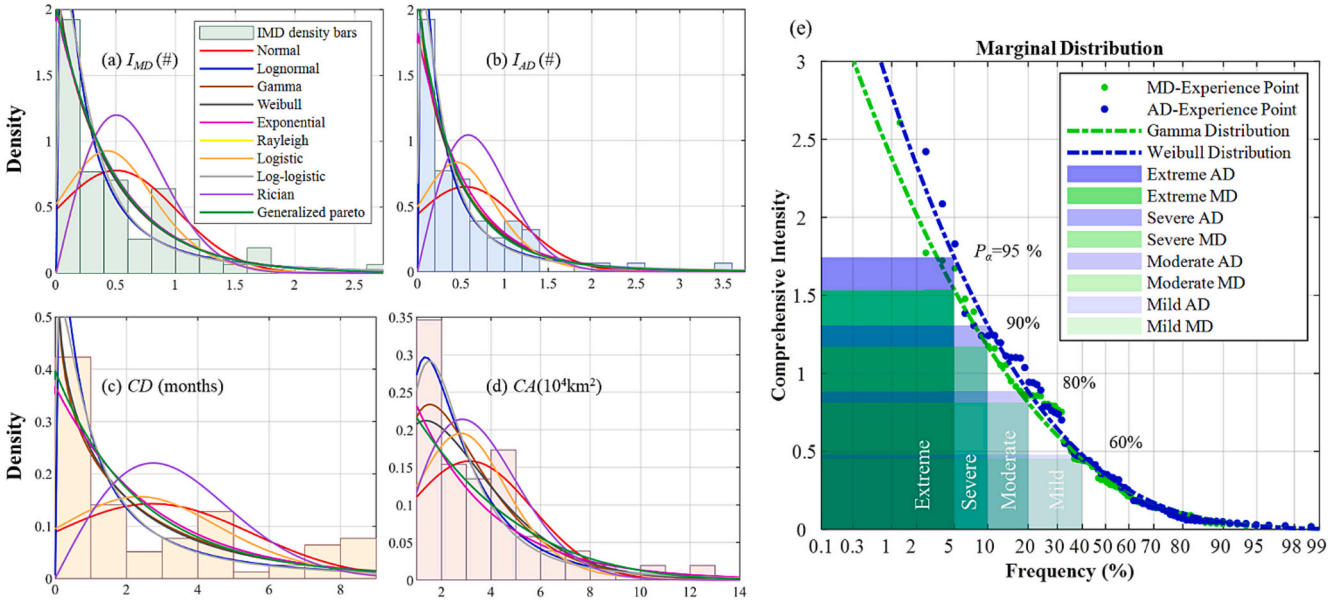

Fig. 9. Fitting results of marginal distributions for (a) I_{MD}, (b) I_{AD}, (c) *CD*, and (d) CA. (e) Drought levels determined based on the percentiles of marginal distribution.

distribution from ~10 different distributions to fit the marginal distributions, these prior assumptions may cause biases in the probability calculations of the Vine copula model (Apurv and Cai, 2019). More complex models such as mixture models or non-parametric models can be used to fit the marginal distributions. The application of other Vine copula types, such as D-Vine copulas, and asymmetric Archimedean copulas will be investigated in future work, broadening the scope of our analysis.

3.4.2. Drought ranking based on comprehensive intensity

Drought events are ranked into different intensity levels, such as extreme, severe, moderate, mild, and slight, reflecting varying degrees of drought impact (Shi et al., 2018). The percentile method quantifies the rarity of drought events occurring in history and can be used to classify drought levels (Zhang et al., 2023). In this study, the extreme drought level was determined by the 95th percentile (P_α = 95 %) of marginal distribution of the comprehensive intensity, while the severe, moderate, and mild drought levels were determined by the 90th, 80th, and 60th percentiles, respectively. Fig. 9e illustrates the empirical frequency points and comprehensive intensity intervals of drought events at different levels. Table 5 summarizes the lower critical thresholds for I_{MD} or I_{AD} of drought events under each level. For instance, drought events with $I_{MD} \geq 1.53$ and $I_{AD} \geq 1.74$ were considered extreme meteorological drought (Extreme MD) and extreme agricultural drought (Extreme AD) events respectively, and so on. The I_{MD} thresholds across all levels exceed the I_{AD} thresholds, predominantly because agricultural droughts had, within the study period, been more frequent than meteorological droughts.

3.4.3. Vine copula-based propagation probability and model validation

Conditional probability contributes valuable insights for effective allocation of water resources under specific drought conditions (Guo et al., 2020). To ascertain the probabilities of triggering different agricultural drought levels under distinct meteorological drought intensities and specific propagation potentials, Vine Copula model for coupled spatiotemporal features was employed. Combined with the four I_{AD} thresholds (extreme, severe, moderate and mild) in Table 5, the model evaluated the exceedance probabilities of these drought levels in CY under I_{MD}, *CD*, and *CA* accumulations to certain levels, as depicted in Fig. 10. For instance, when $I_{MD} \geq 2.0 \cap CD \geq 4.5$ (months) $\cap$ $CA \geq 5.0$ (10^4 km^2), an extreme meteorological drought and high propagation potential condition, the probability of triggering an extreme agricultural drought ($I_{AD} \geq 1.74$) was 46.84 %, while the likelihood of inciting a severe ($I_{AD} \geq 1.31$), moderate ($I_{AD} \geq 0.88$), and mild ($I_{AD} \geq 0.48$) agricultural drought was 62.34 %, 76.46 %, and 97.03 %, respectively.

Probabilistic analysis revealed a distinct "stratification" phenomenon of the compound duration (*CD*) on agricultural drought. Primarily attributed to the significant upper-tail correlation between *CD* and I_{MD}. For instance, extreme agricultural drought (Fig. 10a) exhibited a fluctuating probability within 3–6 months of *CD*. However, the probability of extreme agricultural drought was virtually zero when *CD* was <3 months, regardless of variations in I_{MD} or CA. Nevertheless, even with low intensity, the probability of extreme agricultural drought remains high when $CD \geq 5$ (months), which should not be overlooked in agricultural drought management. This indicates that the occurrence of agricultural drought necessitates a certain accumulation duration, making early prevention and control measures during the propagation period the optimal time for issuing drought warnings and implementing regulatory actions. Under specific spatiotemporal coupling index (*f*), I_{MD} was fundamental driver of agricultural drought. For example, for moderate agricultural drought (Fig. 10c), propagation probability increased with escalating I_{MD}.

Traditional method of propagation probability only considers one aspect of drought characteristics, such as intensity (Fig. 10e), and neglects the spatiotemporal conditions of propagation. Even if the intensity, duration, and area of meteorological drought are included in high-dimensional modeling (Zhang et al., 2021), it cannot fully reflect the cumulative effect of drought propagation in time and space. Relying solely on univariate meteorological drought features is inadequate for accurately estimating propagation likelihood (Won et al., 2020). Due to neglect of spatiotemporal information, bivariate copula underestimated the propagation probability of meteorological drought with the characteristics of "low-I_{MD} but long-*CD*" or "low-I_{MD} but large-*CA*", while overestimated the propagation probability of meteorological drought with the characteristics of "high-I_{MD} but short-*CD* and small-*CA*". For example, the binary copula indicated that the probability of an extreme meteorological drought causing an extreme agricultural drought was 31.29 % (Fig. 10e). In contrast, Fig. 11a shows the probability distribution cross-section of *CD* and *CA* jointly triggering an extreme agricultural drought ($I_{AD} \geq 1.74$) under extreme meteorological drought conditions ($I_{MD} = 1.53$). Results showed that when $CD = 5$ (months) $\cap$ $CA \geq 4.5$ (10^4 km^2), the probability was basically close 31.29 %. However, when $CD \leq 4$ (months), this probability was overestimated (because it was difficult for area *A* to cause extreme agricultural drought), and when $CD \geq 6$ (months) and *CA* was large, this probability was underestimated (because area *B* had a high potential for causing extreme agricultural drought). Area *A* was defined as a low-risk area for the propagation of extreme agricultural drought, which was mainly limited by *CD*, and the time cumulative effect was not significant. Area *B* was a high-risk area for propagation, mainly due to *CD*, and the risk was higher as *CA* increases.

From compound drought perspective, drought propagation was a slow accumulation process, where I_{MD} was the external driving factor, and *CD* and *CA* respectively represented the cumulative scale of propagation in time and space. Under compound drought scenarios, the individual coupling characteristics may not be extreme themselves, but their co-occurring result in a cascading impact, leading to a significant increase in propagation probability. Therefore, expanding the temporal and spatial connotations of drought propagation by considering propagation conditions (i.e., *CD* and *CA*) helped mitigate errors or uncertainties arising from solely focusing on meteorological intensity when assessing agricultural drought, providing new insights for agricultural disaster management.

To validate the robustness of the model and investigate the correlation between variables, conditional sampling based on original dataset was performed to provide a visual goodness-of-fit test (Sharma and Mujumdar, 2022). The resulting samples were overlaid onto the scatterplot along with the original data (Fig. 11b). It is evident that the simulated generations (blue dots) offer good coverage of the original data (gray dots), suggesting that the Vine copula model can capture the dependencies in the original observations. Besides the concurrence in univariate, the co-variability between the generated and observed pairs demonstrated consistency, indicating that the fitted Vine copula reasonably represented a realistic interdependence among relevant physical processes while employing appropriate marginal distributions.

Table 5
Critical intensity thresholds of drought events at different levels.

Drought rank	Extreme	Severe	Moderate	Mild
Percentile (%)	95	90	80	60
Frequency (%)	5	10	20	40
I_{MD}	1.53	1.17	0.81	0.45
I_{AD}	1.74	1.31	0.88	0.48

4. Conclusions

To understand the spatiotemporal propagation of drought, this study presents a novel approach using Vine copula for coupling spatiotemporal features to evaluate drought propagation in compound drought scenarios. Firstly, 3D identification method was employed for meteorological and agricultural drought events, constructing comprehensive

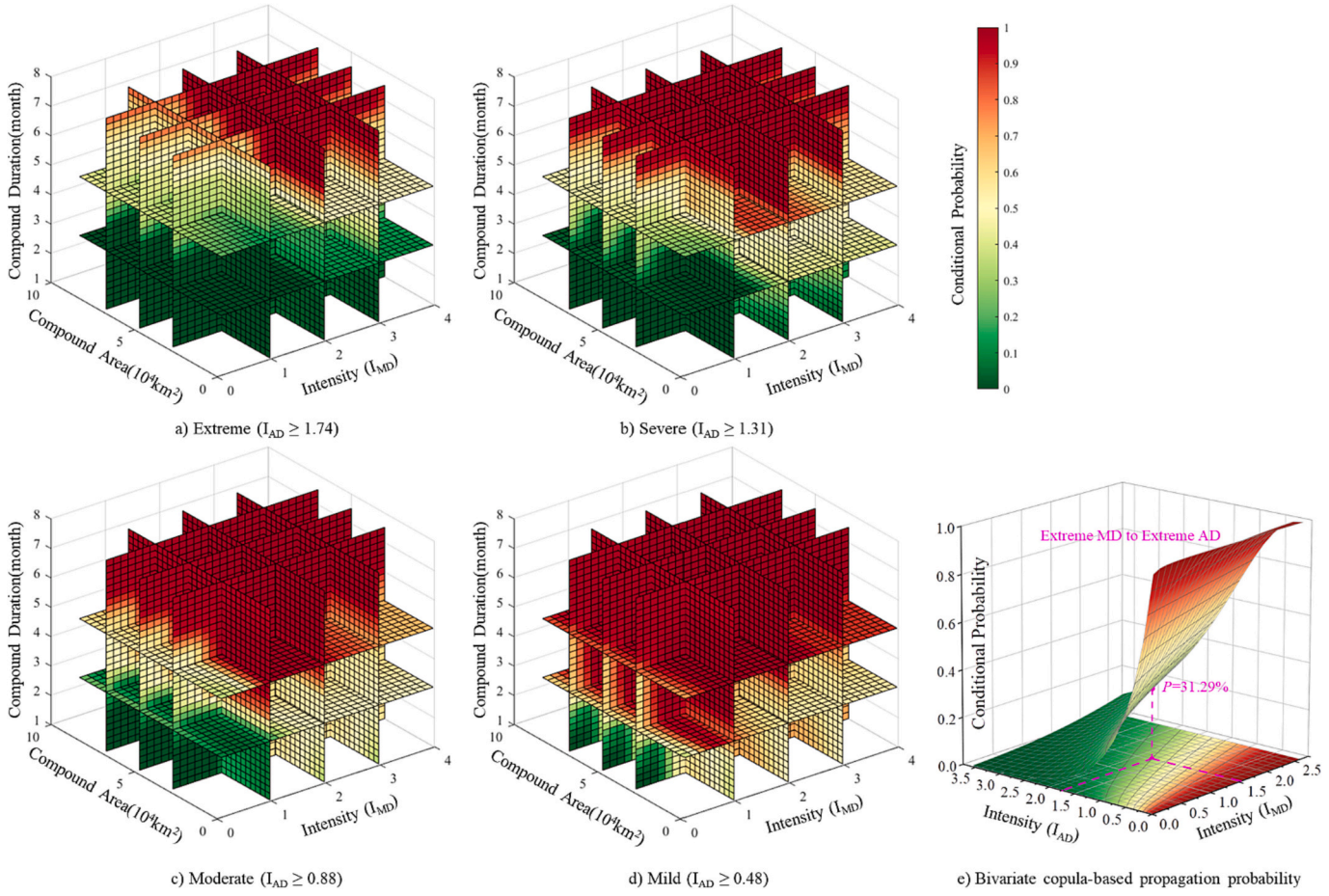

Fig. 10. The conditional probability of triggering (a) extreme, (b) severe, (c) moderate, and (d) mild agricultural drought under given I_{MD}, *CD*, and CA. (e) Bivariate copula propagation probability without *CD* and CA.

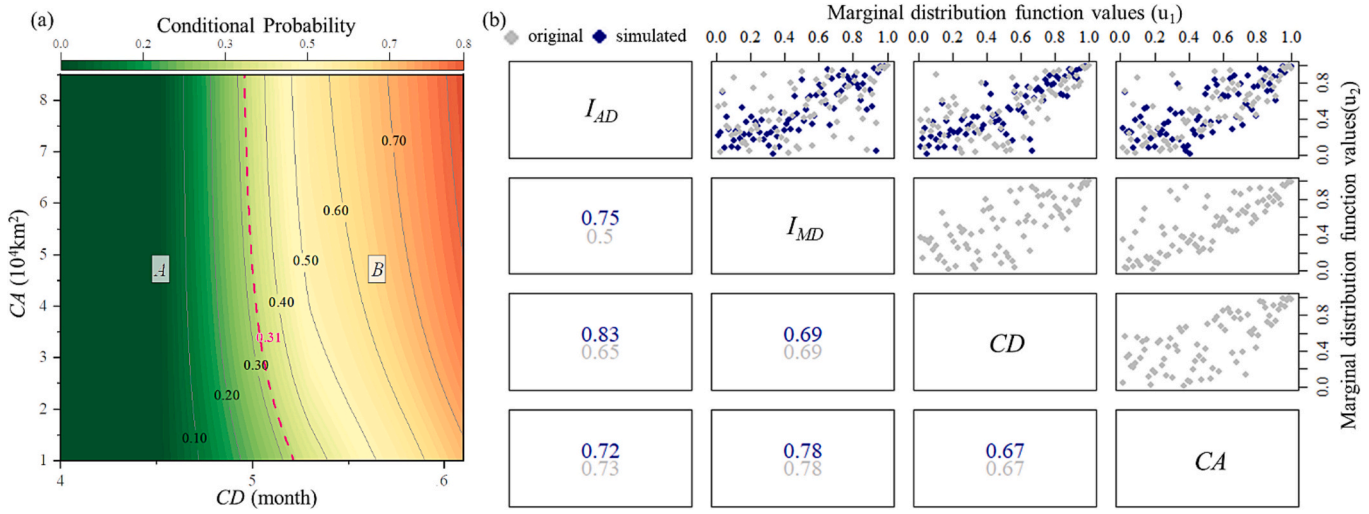

Fig. 11. (a) Probability distribution of *CD* and *CA* triggering extreme agricultural drought ($I_{AD} \geq 1.74$) under extreme meteorological drought conditions ($I_{MD} = 1.53$). (b) Pairwise dependencies among the four coupling characteristics using conditional simulation.

intensity metrics (I_{MD} and I_{AD}) for these two types of drought events. Subsequently, through matching criteria, compound drought events were extracted from the meteorological-agricultural drought event pairs, and the *CD* and *CA* were obtained, which characterize spatio-temporal propagation potential. Furthermore, the dependence relationships were elucidated among four key features (I_{MD}, *CD*, *CA* and I_{AD}). Finally, Vine copula was used to couple the four variables and evaluate the probability of triggering agricultural drought with different intensity levels. Main conclusions are as follows:

1) The 3D identification method was effective in detecting minor drought events. It allowed for capturing the multi-dimensional

characteristics of drought from a continuous spatiotemporal perspective. The comprehensive intensity took into account the nonlinear relationship between drought duration, area, and severity, representing a new method for drought characteristic measurement.

2) Based on the principle of spatial-temporal overlap, the majority of high-intensity drought events were successfully matched. A total of 78 meteorological-agricultural drought event pairs (*M-A*-78) were assembled in CY. Meteorological drought triggers agricultural drought through distinct spatiotemporal cumulative effects. Drought propagation potential can be characterized by their spatiotemporal intersection, i.e., *CD* and CA.
3) Correlation analysis indicated that *CD* and *CA* encompasses probability information pertaining to subsequent agricultural drought. I_{MD} spread to I_{AD} through a special "channel", and *CD* and *CA* played a crucial role as the bridge in this propagation process. Overall migration and evolution patterns of meteorological and agricultural droughts in CY were consistent (SE → NW). Drought characteristics existed a profound spatiotemporal relationship.
4) According to the percentiles of marginal distribution, the critical thresholds for different levels of drought events were determined. Based on constructed Vine copula-based propagation probability model, we can intuitively determine the probability of agricultural drought occurrence under different meteorological conditions and propagation potential. At a certain I_{MD} level, *CD* significantly influences the probability of propagation (i.e., "stratification" phenomenon), while *CA* also increases the probability of propagation proportionally.
5) Individual drought characteristics may not be extreme themselves, but their co-occurring result in a cascading impact, leading to a significant increase in propagation probability. Probability evaluation lacking spatiotemporal propagation information may underestimate the probability of meteorological drought propagation characterized by "low-I_{MD} but long-*CD*" or "low-I_{MD} but large-*CA*". The developed Vine copula model can effectively capture the dependence structure between coupling characteristics, and exhibits reliable robustness.

In summary, this study proposed a propagation probability model of coupled spatiotemporal features, which was used to calculate the probability of triggering agricultural drought with different severity levels under compound drought scenarios. By considering both meteorological conditions and propagation potential, this research offers several advantages over existing methods, including the ability to capture the spatiotemporal information of propagation, and to provide more accurate and comprehensive evaluation of agricultural drought risks. The spatiotemporal matching approach is applicable to pair different types of droughts and has the potential to be extended to other types of droughts, such as hydrological droughts and ecological droughts. However, this study had some limitations. FLDAS was the single data source used, and the sample size of drought events was limited to only a few dozen data points, leading to uncertainty in the estimation of multivariate distributions using the Vine copula model. Additionally, the sensitivity of *CD* and *CA* are associated with the spatiotemporal scales of drought, which represent distinct dryness/wetness conditions. This study mainly focused on monthly drought characteristics and may overlook the impact of large-scale and rapid-onset drought, such as global flash drought. In future research, the limitations will be addressed to enhance and compare probability assessments.

CRediT authorship contribution statement

Guibin Yang: Writing – original draft, Visualization, Methodology, Conceptualization. **Jianxia Chang:** Validation, Supervision, Data curation. **Yimin Wang:** Resources, Project administration. **Aijun Guo:** Validation, Formal analysis. **Lu Zhang:** Visualization. **Kai Zhou:** Software. **Zhenwei Wang:** Validation.

Declaration of competing interest

The authors declare no conflicts of interest relevant to this study.

Data availability

Monthly FLDAS data for precipitation and soil moisture are acquired from NASA Goddard Earth Science Data and Information Service Center (GES DISC; https://disc.gsfc.nasa.gov/datasets?keywords=FLDAS). The original data & program used in the study are available online (https://www.scidb.cn/s/Mruq6r).

Acknowledgments

The authors gratefully acknowledge the editor and anonymous reviewers for their constructive comments and suggestions improving this manuscript. This research was jointly funded by the National Key R&D Program of China (grant number 2021YFC3000203).

References

AghaKouchak, A., Chiang, F., Huning, L.S., Love, C.A., Mallakpour, I., Mazdiyasni, O., et al., 2020. Climate extremes and compound hazards in a warming world. Annu. Rev. Earth Planet. Sci. 48, 519–548.
Apurv, T., Cai, X., 2019. Evaluation of the stationarity assumption for meteorological drought risk estimation at the multidecadal scale in contiguous United States. Water Resour. Res. 55, 5074–5101.
Apurv, T., Sivapalan, M., Cai, X., 2017. Understanding the role of climate characteristics in drought propagation. Water Resour. Res. 53, 9304–9329.
Ayantobo, O.O., Wei, J., Wang, G., 2021. Modeling joint relationship and design scenarios between precipitation, surface temperature, and atmospheric precipitable water over mainland China. EARTH AND SPACE SCIENCE 8.
Biondi, F., Meko, D.M., 2019. Long-term hydroclimatic patterns in the Truckee-Carson basin of the Eastern Sierra Nevada, USA. Water Resour. Res. 55, 5559–5574.
Chang, J., Li, Y., Wang, Y., Yuan, M., 2016. Copula-based drought risk assessment combined with an integrated index in the Wei River Basin, China. J. Hydrol. 540, 824–834.
Crausbay, S.D., Ramirez, A.R., Carter, S.L., Cross, M.S., Hall, K.R., Bathke, D.J., et al., 2017. Defining ecological drought for the twenty-first century. Bull. Am. Meteorol. Soc. 98, 2543–2550.
Dobson, B., Coxon, G., Freer, J., Gavin, H., Mortazavi-Naeini, M., Hall, J.W., 2020. The spatial dynamics of droughts and water scarcity in England and Wales. Water Resour. Res. 56.
Eltahir, E.A.B., Yeh, P.J.-F., 1999. On the asymmetric response of aquifer water level to floods and droughts in Illinois. Water Resour. Res. 35, 1199–1217.
Farrokhi, A., Farzin, S., Mousavi, S.-F., 2021. Meteorological drought analysis in response to climate change conditions, based on combined four-dimensional vine copulas and data mining (VC-DM). J. Hydrol. 603.
Feng, S., Hao, Z., Zhang, X., Hao, F., 2019. Probabilistic evaluation of the impact of compound dry-hot events on global maize yields. Sci. Total Environ. 689, 1228–1234.
Gao, Y., Zhao, T., Tu, T., Tian, Y., Zhang, Y., Liu, Z., et al., 2024. Spatiotemporal links between meteorological and agricultural droughts impacted by tropical cyclones in China. Sci. Total Environ. 912, 169119.
Guo, Y., Huang, S., Huang, Q., Leng, G., Fang, W., Wang, L., et al., 2020. Propagation thresholds of meteorological drought for triggering hydrological drought at various levels. Sci. Total Environ. 712, 136502.
Jaranilla-Sanchez, P.A., Wang, L., Koike, T., 2011. Modeling the hydrologic responses of the Pampanga River basin, Philippines: a quantitative approach for identifying droughts. Water Resour. Res. 47.
Jehanzaib, M., Sattar, M.N., Lee, J.-H., Kim, T.-W., 2020. Investigating effect of climate change on drought propagation from meteorological to hydrological drought using multi-model ensemble projections. Stoch. Env. Res. Risk A. 34, 7–21.
Jiang, T., Su, X., Zhang, G., Zhang, T., Wu, H., 2023. Estimating propagation probability from meteorological to ecologicaldroughts using a hybrid machine learning copula method. Hydrol. Earth Syst. Sci. 27, 559–576.
Kanthavel, P., Saxena, C.K., Singh, R.K., 2022. Integrated drought index based on vine copula modelling. Int. J. Climatol. 42, 9510–9529.
Kao, S.-C., Govindaraju, R.S., 2010. A copula-based joint deficit index for droughts. J. Hydrol. 380, 121–134.
Li, W., El-Askary, H., Thomas, R., Tiwari, S.P., Manikandan, K.P., Piechota, T., et al., 2020. An assessment of the hydrological trends using synergistic approaches of remote sensing and model evaluations over global arid and semi-arid regions. Remote Sens. 12.
Lin, Q., Wu, Z., Zhang, Y., Peng, T., Chang, W., Guo, J., 2023a. Propagation from meteorological to hydrological drought and its application to drought prediction in the Xijiang River basin, South China. J. Hydrol. 617, 128889.

Lin, Q., Wu, Z., Zhang, Y., Peng, T., Chang, W., Guo, J., 2023b. Propagation from meteorological to hydrological drought and its application to drought prediction in the Xijiang River basin, South China. J. Hydrol. 617.
Liu, Y., Zhu, Y., Ren, L., Singh, V.P., Yong, B., Jiang, S., et al., 2019. Understanding the spatiotemporal links between meteorological and hydrological droughts from a three-dimensional perspective. J. Geophys. Res.-Atmos. 124, 3090–3109.
Liu, Y., Ding, Z., Chen, Y.A., Yan, F.Q., Yu, P.J., Man, W.D., et al., 2023a. Restored vegetation is more resistant to extreme drought events than natural vegetation in Southwest China. Sci. Total Environ. 866.
Liu, Y., Shan, F., Yue, H., Wang, X., 2023b. Characteristics of drought propagation and effects of water resources on vegetation in the karst area of Southwest China. Sci. Total Environ. 891.
Liu, Y., Shan, F., Yue, H., Wang, X., Fan, Y., 2023c. Global analysis of the correlation and propagation among meteorological, agricultural, surface water, and groundwater droughts. J. Environ. Manag. 333, 117460.
Liu, Y., Yu, X., Dang, C., Yue, H., Wang, X., Niu, H., et al., 2023d. A dryness index TSWDI based on land surface temperature, sun-induced chlorophyll fluorescence, and water balance. ISPRS J. Photogramm. Remote Sens. 202, 581–598.
Lloyd-Hughes, B., 2012. A spatio-temporal structure-based approach to drought characterisation. Int. J. Climatol. 32, 406–418.
Lu, E., Zhao, W., Gong, L., Chen, H., Wang, H., Li, X., et al., 2015. Determining starting time and duration of extreme precipitation events based on intensity. Clim. Res. 63, 31–41.
Lu, E., Zhao, W., Zou, X., Ye, D., Zhao, C., Zhang, Q., 2017. Temporal-spatial monitoring of an extreme precipitation event: determining simultaneously the time period it lasts and the geographic region it affects. J. Clim. 30, 6123–6132.
Ma, S., Zhang, S., Wang, N., Huang, C., Wang, X., 2021. Prolonged duration and increased severity of agricultural droughts during 1978 to 2016 detected by ESA CCI SM in the humid Yunnan Province, Southwest China. CATENA 198, 105036.
Mallya, G., Tripathi, S., Govindaraju, R.S., 2015. Probabilistic drought classification using gamma mixture models. J. Hydrol. 526, 116–126.
McKee, T.B., Doesken, N.J., Kleist, J., American Meteorological, S., 1995. Drought monitoring with multiple time scales. In: 9th Conference, Applied Climatology. The Society, Dallas; TX, pp. 233–236.
McNally, A., Jacob, J., Arsenault, K., Slinski, K., Sarmiento, D.P., Hoell, A., et al., 2022. A Central Asia hydrologic monitoring dataset for food and water security applications in Afghanistan. Earth System Science Data 14, 3115–3135.
Mishra, A.K., Ines, A.V.M., Das, N.N., Khedun, C.P., Singh, V.P., Sivakumar, B., et al., 2015. Anatomy of a local-scale drought: application of assimilated remote sensing products, crop model, and statistical methods to an agricultural drought study. J. Hydrol. 526, 15–29.
Ni, L., Wang, D., Wu, J., Wang, Y., Tao, Y., Zhang, J., et al., 2020. Vine copula selection using mutual information for hydrological dependence modeling. Environ. Res. 186.
Nikraftar, Z., Mostafaie, A., Sadegh, M., Afkueieh, J.H., Pradhan, B., 2021. Multi-type assessment of global droughts and teleconnections. Weather and Climate Extremes 34.
Novick, K.A., Ficklin, D.L., Stoy, P.C., Williams, C.A., Bohrer, G., Oishi, A.C., et al., 2016. The increasing importance of atmospheric demand for ecosystem water and carbon fluxes. Nat. Clim. Chang. 6, 1023–1027.
Pascolini-Campbell, M., Reager, J.T., Chandanpurkar, H.A., Rodell, M., 2021. RETRACTED ARTICLE: a 10 per cent increase in global land evapotranspiration from 2003 to 2019. Nature 593, 543–547.
Rulinda, C.M., Dilo, A., Bijker, W., Stein, A., 2012. Characterising and quantifying vegetative drought in East Africa using fuzzy modelling and NDVI data. J. Arid Environ. 78, 169–178.
Rulinda, C.M., Stein, A., Turdukulov, U.D., 2013. Visualizing and quantifying the movement of vegetative drought using remote-sensing data and GIS. Int. J. Geogr. Inf. Sci. 27, 1481–1496.
Sharma, S., Mujumdar, P.P., 2022. Modeling concurrent hydroclimatic extremes with parametric multivariate extreme value models. Water Resour. Res. 58.
Shi, H., Chen, J., Wang, K., Niu, J., 2018. A new method and a new index for identifying socioeconomic drought events under climate change: a case study of the East River basin in China. Sci. Total Environ. 616-617, 363–375.
Shi, H., García-Reyes, M., Jacox, M.G., Rykaczewski, R.R., Black, B.A., Bograd, S.J., et al., 2021. Co-occurrence of California drought and Northeast Pacific marine heatwaves under climate change. Geophys. Res. Lett. 48, e2021GL092765.
Singh, J., Ashfaq, M., Skinner, C.B., Anderson, W.B., Mishra, V., Singh, D., 2022. Enhanced risk of concurrent regional droughts with increased ENSO variability and warming. Nat. Clim. Chang. 12, 163–+.
Sklar, M., 1959. Fonctions de répartition à N dimensions et leurs marges. Annales de l'ISUP VIII 229–231.
Thong, N.-H., Deo, R.C., Mushtaq, S., Kath, J., Khan, S., 2019. Copula statistical models for analyzing stochastic dependencies of systemic drought risk and potential adaptation strategies. Stoch. Env. Res. Risk A. 33, 779–799.
Tian, F., Yang, J., Liu, L., Wu, J., 2022. Progress of research on the conception, characteristic, and influencing factors of drought propagation from the perspective of geographic sciences. Prog. Geogr. 41, 173–184.
Tripathy, K.P., Mishra, A.K., 2023. How unusual is the 2022 European compound drought and heatwave event? Geophys. Res. Lett. 50.
Van Loon, A.F., 2015. Hydrological drought explained. WIREs Water 2, 359–392.
Vogel, J., Paton, E., Aich, V., Bronstert, A., 2021. Increasing compound warm spells and droughts in the Mediterranean Basin. Weather and Climate Extremes 32, 100312.
Walker, D.W., Van Loon, A.F., 2023. Droughts are coming on faster. Science 380, 130–132.
Wang, Y., Yuan, X., 2022. Land-atmosphere coupling speeds up flash drought onset. Sci. Total Environ. 851, 158109.
Wang, M., Ding, Z., Wu, C., Song, L., Ma, M., Yu, P., et al., 2021. Divergent responses of ecosystem water-use efficiency to extreme seasonal droughts in Southwest China. Sci. Total Environ. 760.
Wang, Y., Wang, Y., Chen, Y., Chen, H., Li, X., Ding, Z., et al., 2023. Spatial and temporal characteristics of drought events in Southwest China over the past 120 years. Remote Sens. 15.
Weng, Z., Niu, J., Guan, H., Kang, S., 2023. Three-dimensional linkage between meteorological drought and vegetation drought across China. Sci. Total Environ. 859.
Won, J., Choi, J., Lee, O., Kim, S., 2020. Copula-based joint drought index using SPI and EDDI and its application to climate change. Sci. Total Environ. 744.
Wu, H., Su, X., Singh, V.P., Feng, K., Niu, J., 2021. Agricultural drought prediction based on conditional distributions of vine copulas. Water Resour. Res. 57.
Wu, J., Yao, H., Chen, X., Wang, G., Bai, X., Zhang, D., 2022. A framework for assessing compound drought events from a drought propagation perspective. J. Hydrol. 604.
Wu, C., Zhong, L., Yeh, P.J.F., Gong, Z., Lv, W., Chen, B., et al., 2024. An evaluation framework for quantifying vegetation loss and recovery in response to meteorological drought based on SPEI and NDVI. Sci. Total Environ. 906, 167632.
Xu, X., Tang, Q., 2021. Spatiotemporal variations in damages to cropland from agrometeorological disasters in mainland China during 1978–2018. Sci. Total Environ. 785, 147247.
Xu, Y., Zhang, X., Hao, Z., Singh, V.P., Hao, F., 2021. Characterization of agricultural drought propagation over China based on bivariate probabilistic quantification. Journal of Hydrology 598.
Yoo, J., Kim, J., Kwon, H.-H., Kim, T.-W., 2022. A new drought monitoring approach using three-dimensional drought properties based on a dynamic drought detection technique algorithm. Journal of Hydrology-Regional Studies 44.
Yu, T., Jiapaer, G., Bao, A., Zhang, J., Tu, H., Chen, B., et al., 2023. Evaluating surface soil moisture characteristics and the performance of remote sensing and analytical products in Central Asia. J. Hydrol. 617.
Zhang, T., Su, X., Feng, K., 2021. The development of a novel nonstationary meteorological and hydrological drought index using the climatic and anthropogenic indices as covariates. Sci. Total Environ. 786.
Zhang, Q., Shi, R., Singh, V.P., Xu, C.-Y., Yu, H., Fan, K., et al., 2022a. Droughts across China: drought factors, prediction and impacts. Sci. Total Environ. 803.
Zhang, X., Hao, Z., Singh, V.P., Zhang, Y., Feng, S., Xu, Y., et al., 2022b. Drought propagation under global warming: characteristics, approaches, processes, and controlling factors. Sci. Total Environ. 838.
Zhang, Y., You, Q., Ullah, S., Chen, C., Shen, L., Liu, Z., 2023. Substantial increase in abrupt shifts between drought and flood events in China based on observations and model simulations. Sci. Total Environ. 876.
Zhou, S., Williams, A.P., Berg, A.M., Cook, B.I., Zhang, Y., Hagemann, S., et al., 2019. Land-atmosphere feedbacks exacerbate concurrent soil drought and atmospheric aridity. Proc. Natl. Acad. Sci. USA 116, 18848–18853.
Zhou, K., Wang, Y.M., Chang, J.X., Zhou, S., Guo, A.J., 2021. Spatial and temporal evolution of drought characteristics across the Yellow River basin. Ecol. Indic. 131.
Zhu, Y., Liu, Y., Wang, W., Singh, V.P., Ren, L., 2021. A global perspective on the probability of propagation of drought: from meteorological to soil moisture. J. Hydrol. 603.
Zscheischler, J., Fischer, E.M., 2020. The record-breaking compound hot and dry 2018 growing season in Germany. Weather and Climate Extremes 29.